WEP Warwick Evans Publishing

International Journal of Materials Science and Technology Studies

ISSN: 3006-7693 (Print), ISSN: 3006-3744 (Online) | Volume 3, Number 1, Year 2025
DOI: https://doi.org/10.62051/ijmsts.v3n1.05
Journal homepage: https://wepub.org/index.php/IJMSTS/index

Study of Shaped Shapes of Cellulose Acetate Films Based on Mie Scattering

Chenbo Zhi [1], Yihan Zhang [2], Yingqin Shi [3], Xiaoyu Zhou [1], Fengjia Sun [1]

[1] School of Physical Science and Technology, Tiangong University, Tianjin 300387, China

[2] School of Computer Science and Technology, Tiangong University, Tianjin 300387, China

[3] School of Electronic Information and Engineering, Tiangong University, Tianjin 300387, China

ABSTRACT

The emerging cellulose acetate film is also a composite material with excellent cooling properties due to its excellent flexibility and good film-forming properties, and nowadays it has become a key material used for radiation cooling. Since the cross-section of the columnar skeleton of cellulose acetate film is irregular and heterogeneous, which is not the traditional circular shape, at present, domestic and foreign research mainly analyses the circular shape, and does not explore the influence of the heterogeneous shape on the scattering effect of cellulose acetate film in depth. Therefore, in this paper, through the Mie scattering formula, the complex refractive index of cellulose acetate film in actual measurement is substituted into the formula for the simulation of scattering efficiency, extinction efficiency, absorption efficiency and backward scattering efficiency factor of the particles, and on the basis of this, different size parameters of the particles are simulated to obtain the relationship between the scattering direction of the particles and the size parameters. After that, the heteromorphic shape was modelled and simulated based on the Fourier formula in polar coordinates, which was substituted into the simulation software for comparing the light scattering cross section of the heteromorphic shape with that of the traditional circular shape, and then the heteromorphic shape was adjusted and optimized on the basis of the same cellulose acetate film. It is found that the heteromorphic shape has a larger surface area than a circle, and its special shape can form an asymmetric radiation route, which can scatter the light emitted from the side better, thus providing a feasible graphical solution for the preparation of cellulose acetate radiation-cooled films.

KEYWORDS

Cellulose acetate; Mie scattering; Heteromorphic shape; Scattering efficiency; Backscattering efficiency factor

1. INTRODUCTION

1.1. Background of the Project Study

Climate change due to global warming has become one of the serious challenges facing the world in the 21st century. Traditional cooling methods use active refrigeration equipment to achieve cooling, which not only causes a large amount of energy consumption, but also leads to an increase in greenhouse gas emissions, thus forming a vicious cycle. Compared with the traditional active cooling method, radiant cooling does not require the burning of fossil fuels and does not emit pollutants, combining the advantages of being green and sustainable. China's commitment to strive to achieve ‘carbon peak’ before 2030, 2060 to achieve ‘carbon neutral’, radiation refrigeration can better achieve sustainable development of mankind, which not only responds to the call of China to achieve the ‘dual-carbon’ goal, but also to achieve the ‘dual-carbon’ goal. This not only responds to China's call

to achieve the ‘dual-carbon’ goal, but also conforms to the global emphasis on low-carbon environmental protection development trend.

1.2. Current Research Status of Radiation Refrigeration

1.2.1. Radiation cooling principle

According to Planck's law, the terrestrial radiation with a temperature of 300 K on the surface of the earth is concentrated in the wavelength range of 2.5 to 50. The temperature of the universe is about 3K, so the earth's surface can take advantage of the huge temperature difference through the atmosphere to the universe to emit thermal infrared radiation to achieve refrigeration. The atmosphere is a semi-transparent medium, mainly composed of oxygen, nitrogen and other gases, which can absorb, emit and scatter electromagnetic waves, and its radiation characteristics are related to the wavelength. The temperature of the sun's surface is about 5,800 K. The heat of objects on Earth comes mainly from solar radiation. Since the Earth is tightly wrapped by the atmosphere, when direct sunlight, part of the electromagnetic waves will pass through the atmosphere directly to the Earth's surface, while most of them will be absorbed, reflected and scattered by the atmosphere, and part of the scattered part will be scattered to outer space, and the other part will be scattered to the Earth's surface. The atmosphere reflects, scatters or absorbs most of these electromagnetic waves, but exhibits high transmittance in certain infrared bands called atmospheric windows, where the wavelengths of peak thermal radiation at typical ambient temperatures (~300 K) are consistent with the atmospheric windows, according to Wien's displacement law. Therefore, under the right atmospheric conditions, a surface with the right thermal radiation characteristics can radiate heat into outer space at a temperature of only 3 K and achieve radiative cooling.

Radiation refrigeration is a kind of thermal radiation to rely on the object's own heat in the form of electromagnetic waves to the outer space cooling technology is essentially a radiator and the environment between the radiant heat exchange, involving solar radiation, infrared atmospheric radiation and the influence of the material thermal radiation.

Radiation refrigeration technology makes full use of the low-temperature cold source characteristics of outer space, mainly using the atmosphere in the ‘atmospheric window’ band (8-13μm) of the high permeability of the heat of the Earth's surface in the form of thermal radiation to the low-temperature loss of outer space, so as to achieve passive refrigeration effect. Thermal radiation is an important way of exchanging heat between objects. When the surface temperature of an object is greater than 0 K, it radiates heat to the surrounding environment and receives radiant energy from other objects in the environment at the same time. Therefore, when there is a heat difference between objects, the phenomenon of high heat objects radiating heat to low heat objects will occur. The temperature of outer space is about 3 K, and the temperature of the Earth's surface is about 300 K. Therefore, it is possible to use the huge temperature difference between the Earth's surface and outer space to exchange heat to achieve the cooling effect.

The whole mechanism of radiative cooling can be regarded as a simple energy balance process, where P_{rad} represents the thermal radiation on the surface of the radiator, P_{solar} represents the absorbed solar radiation, P_{atm} represents the absorbed atmospheric radiation, and $P_{non-radiative}$ represents the non-radiation loss and heat exchange or heat convection. According to the energy balance theory, the net radiative cooling power $P_{net-cooling}$ at the surface of the radiator can be expressed as follows:

$$P_{net-cooling} = P_{rad} - P_{atm} - P_{solar} - P_{non-radiative} \quad (1)$$

Below is a graphical demonstration of a simulation of radiative cooling:

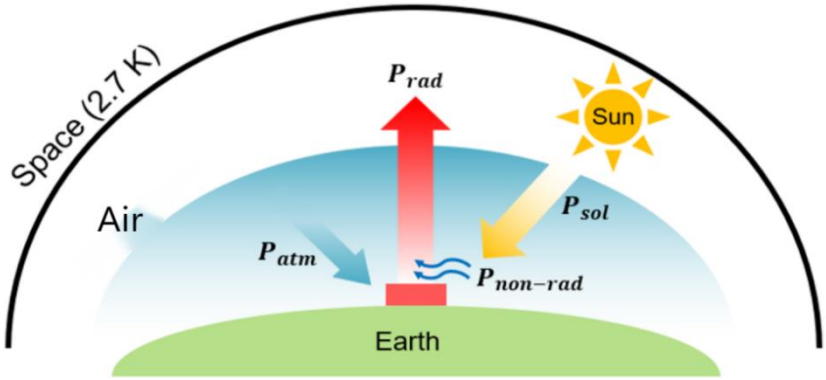

Figure 1. Radiation cooling effect demonstration diagram

1.2.2. Current status of research on radiation-cooled materials

Currently, it is difficult for natural materials to take into account both emissivity and reflectivity requirements, as early studies on radiative cooling mainly focused on the emissive properties of the material itself. It was not until 2014 that Raman et al. made daytime radiative cooling possible by applying photonic structures to radiatively cooled materials for the first time [1].

Currently the materials used for radiative cooling are mainly classified into polymer-based materials, inorganic materials and polymer/inorganic composites. For example, Lv Song, Ji Yishuang [2] et al. proposed an organic composite film of titanium dioxide particles embedded in poly (methyl methacrylate) (PMMA) with simple structure and low cost. The radiative cooling performance of PMMA film was continuously experimented for 24h using a homemade device, and the experimental results showed that the temperature of the radiative cooler could be 11℃ lower than the ambient. Meanwhile Wenjing Lu [3] and others found that the porous films prepared using phase separation method, electrostatic spinning technology, stretching technology which are different preparation methods have different pore structures, and also different modification methods and membrane materials can be used to further improve the performance of the porous films, and the porous films rely on the pore size rejection mechanism, which has a better chemical stability than the traditional IEMs.

However, no matter based on any material, the way to achieve radiation cooling is mainly outward transmission of infrared, reflection of solar radiation and synergistic effect. In recent years, the emergence of nano-optical materials represented by photonic crystals and metamaterials has brought new ideas to the design of optical devices applied to radiation cooling, and the new generation of radiation-cooling devices represented by polymer membrane structures have excellent applicability, permeability, flexibility, and strength, which can easily satisfy the needs of multi-scenario compatibility.

1.3. Advantages of Cellulose Acetate Materials

1.3.1. Advantages of cellulose materials

Yuan Shuaixia [4] of Zhejiang University of Science and Technology in the study of daytime passive radiation refrigeration material natural cellulose-based found that the cellulose membrane has a high reflectance and high emissivity, which means that it has good cooling performance. At the same time cellulose membrane has good hydrophobic properties, which are water and pollution resistant. The hydrophobic cellulose membrane has a water contact angle of 134.0º and is reusable with a long service life. The treated cellulose membrane has an increased pore structure, which helps to improve its spectral properties and gives it a better potential for applications in optics. Cellulose membranes can be used in a number of applications including, but not limited to:

(1) Construction field: cellulose membrane can be used in building exterior walls, roofs and other parts of the building, by reflecting and scattering sunlight, reducing the heat absorption of the building and improving the cooling effect of the building.

(2) solar energy field: cellulose film can be used as a covering layer for solar panels to improve the light absorption efficiency of solar cells.

(3) Optical field: cellulose film can be used to prepare optical filters, mirrors and other optical devices.

1.3.2. Advantages of cellulose acetate based on cellulose synthesis

Cellulose acetate (CA) is a common natural cellulose material with low cost and easy processing, which can be widely used in the preparation of porous films, and cellulose acetate is a renewable natural material with good biocompatibility and degradability, which is friendly to the environment, and it has excellent light transmittance, heat resistance, chemical resistance, and good mechanical properties in physical properties, so it has been widely used in many fields have a wide range of applications. In the field of daytime radiation refrigeration, the porous membrane structure of cellulose acetate can effectively improve the emissivity of the material, so that the object can be more effective in the item of the outer space radiation heat, so as to realize the cooling. In addition, cellulose acetate can achieve high reflectivity to sunlight by adjusting its preparation process and the design of pore structure to meet the regulation of daytime radiative cooling.

Chen Xi [5] from Southeast University used auto-deposited TiO_2 based cellulose acetate porous polymer films as spectrally selective materials for passive daytime radiant cooling is because porous polymers have high void ratio and cellulose acetate has high refractive index, and Jia Jianru [6] from Tianjin Polytechnic University mentioned that the main uses of cellulose acetate films include textile manufacturing, cigarette filter tows and membrane materials. In terms of membrane materials, cellulose acetate membrane has good film-forming properties, high selectivity, high water permeability, simple membrane manufacturing process, good blood compatibility and biocompatibility, etc. It is widely used in seawater purification membranes, osmosis evaporation membranes, dialysis membranes and other fields. Compared with other materials, the advantages of cellulose acetate membrane lie in its flexibility, transparency, good luster, good melt fluidity, easy molding process and thermoplasticity. In addition, cellulose acetate membrane is easily soluble in organic solvents, mild and safe, with good stability and biocompatibility. By changing the spinning parameters, the spinning diameter of cellulose acetate membrane can be controlled, and the ultrafine nanofiber membrane can be prepared and obtained.

1.3.3. Radiative cooling based on cellulose acetate

In previous studies, radiative coolers based on various materials have been gradually proposed, including multilayer structures [7], metamaterials, and porous polymer membrane films [8]. However, conventional radiative cooling devices usually require highly reflective solar substrates, which leads to fabrication complexity and higher costs [9]. Recent studies have shown that generating light-scattering holes in polymers can achieve the same effect as metallic reflectors. In addition, these polymer-based radiative cooling devices have the advantage of low cost and scalable production, making them a promising solution for reducing cooling energy consumption. Whereas cellulose acetate is rich in chemical bonds, such as C-O and C-O-C, and has desirable infrared emissivity in the wavelength range overlapping with the atmospheric transparency window (813μm), it is worth noting that most membranes with radiative cooling capabilities typically exhibit narrow thermal emission, poor water resistance, and poor air permeability. Effective thermal conductivity, perspiration and evaporation properties can be obtained from textile radiative cooling materials.

1.3.4. Application of cellulose acetate radiation cooling

Early on, scientists found that some polymer materials have low reflectivity, low transmittance and high emissivity in the atmospheric transparent window, which can show good radiation cooling effect at night. When irregular nanopores are formed inside the polymer, these micrometer and nanometer-

sized pores can strongly scatter electromagnetic waves of similar wavelengths, and the non-dense pore structure can increase the atomic vibration, which has nearly 96% high reflection of sunlight, and 97% high emission in the infrared wavelengths, and achieves a net cooling power of 96 W/m^2 at a solar irradiance of 890 W/m^2, which can achieve a cooling effect of nearly 6°C during the daytime. Li [10] et al. obtained a porous radiation cooling material by removing lignin from wood and then densifying it. After the lignin is removed from the wood, numerous disordered mesopores will be formed, which can effectively scatter sunlight, and at the same time, the material also has a good emission ability in the infrared region, which is due to the vibration and stretching of cellulose molecules. The cellulose acetate film has numerous micron-nanometer pores that can achieve efficient backscattering and reflection of sunlight, and the rich infrared vibration modes of the cellulose acetate molecules that make up the film make the film have a high mid-infrared emissivity. Cellulose acetate films have high transmittance and radiation absorption in the infrared band. When cellulose acetate film is exposed to the environment, it absorbs thermal radiation from its surroundings, and the molecules in it absorb the radiant energy, which increases its internal thermal energy. By absorbing thermal radiation, the surface temperature of cellulose acetate film decreases. This is because the thermal energy absorbed by the film is transferred to the interior of the film, resulting in a decrease in the surface temperature.

Now, after a long period of research, scientists have explored the application of cellulose acetate in radiative cooling more deeply, and in 2022 a research team from Nanjing University developed a layered cellulose acetate-based radiatively cooled film. The film has broadband and high mid-infrared emissivity, which facilitates high-performance large-scale cooling. Tailored pores act as effective scattering centers for incoming solar radiation, endowing the CA film with high solar reflectivity. Experimental results show that the film achieves a cooling power of up to 110 W/m^2 and a cooling temperature of about 12 °C under direct sunlight, providing an important way to develop effective, mass-producible, and sustainable snow and ice protection. Afterwards, three-dimensional porous composite films were obtained by adding TiO_2 nanoparticles to cellulose acetate (CA) through a simple solvent substitution strategy [11]. Due to the different volatility of solvents, numerous cavities are formed in the cellulose substrate during the volatilization process, and the cavity size is regulated by controlling the rate of solvent volatilization to an average distribution of about 5μm, and according to the Mie scattering theory, the cavities at this size will strongly reflect the sunlight. Meanwhile, TiO_2, as a transition metal oxide with semiconductor properties, exhibits high refractive index and high IR emissivity, etc. The synergistic effect of the introduced TiO2 nanoparticles and the cavity can effectively increase the average solar reflectance to 97%. The actual outdoor test results show that the composite film can still present a cooling effect of about 10°C even under high-density solar radiation (897 W/m^2) conditions [12].

In foreign studies, researchers have proposed a method of dispersing alumina (Al_2O_3) in cellulose acetate and coating it on textiles for human body cooling. Cellulose acetate has high emissivity in the long-wave infrared region (8-13μm), which promotes effective long-wave infrared radiation, while alumina has high thermal conductivity, which enhances solar reflectivity. The solar reflectance of the coated textiles was significantly increased from 62.6% to 80.1% (0.3-2.6μm). Cooling performance experiments showed that this modified textile could reduce the temperature of simulated skin by 2.3-8°C compared to the unmodified reference, and in actual cooling performance experiments, the modified T-shirt reduced the overheating of actual human skin by 0.6-1.0°C, which corresponded to a reduction of the textile's inner surface temperature by 1.9-3.3°C. Subsequently, in 2023, Yuxin Zhang's team Yuxin Zhang's team in 2023 proposed a simple strategy to realize the integration of radiative cooling, radiant heating and active electric heating. Among them, radiative cooling was based only on the self-reflective structure and self-emissive molecular properties of cellulose acetate electrostatically spun film [13]. In the cooling mode, the Janus film reached an average outdoor temperature of 9.4°C lower than that of a commercial cotton fabric.This research opens the way for the development of dynamic thermal regulation technologies. This year Markus Zimmerl et al.

focused on transferring the passive radiative cooling properties of micro- and nanostructures on the body surface of Saharan silver ants to technically available, biodegradable and biomass-based materials. The study successfully transferred the microstructural structural color of CD to a cellulose acetate film and evaluated the reflectance by FTIR spectroscopic measurements, demonstrating that it is feasible to increase the infrared emissivity through surface-induced functionality, thus reducing the surface temperature [14].

1.4. Relationship Between Sunlight Reflection and Radiative Cooling

1.4.1. Effect of sunlight reflection on radiative cooling

Sunlight consists of multiple wavelengths of light, and when sunlight strikes the surface of an object, the surface of the object reflects some of the light. The amount of reflected light depends on the material and color of the object surface. White and smooth surfaces reflect sunlight more, while black and rough surfaces reflect less. By choosing highly reflective materials for the surface of an object, the amount of sunlight absorbed by the object can be reduced, thus lowering the temperature of the object.

There is an interrelated relationship between radiative cooling and sunlight reflection. When sunlight hits the surface of an object, the surface of the object reflects some of the sunlight and absorbs the other part. The absorbed sunlight is converted into heat energy for the object, resulting in an increase in the object's temperature. In order to reduce the temperature of the object, radiative cooling technology can be used to dissipate heat by emitting thermal radiation from the surface of the object to the external space, thus achieving the purpose of cooling. Thus, there is a causal relationship between solar reflection and radiative cooling, i.e., solar reflection reduces the sunlight absorbed by the object and lowers the object temperature, while radiative cooling can further reduce the object temperature by emitting thermal radiation.

In China, Chen Si and Yang Xujie [15] investigated the effect of spectral selectivity of radiative cooling materials on the cooling performance by using spectral analysis and thermal performance testing. Firstly, radiative cooling materials with different spectral selectivity were prepared and their reflectance in sunlight and emissivity in infrared band were tested. Then, the cooling effects of different materials were compared by thermal performance tests. The results show that the radiative cooling materials with high spectral selectivity exhibit better performance in sunlight reflectance and infrared radiation emission, thus improving the cooling effect.

Overseas, there are also some papers that have conducted in-depth research on the relationship between solar reflection and radiative cooling. In the research results of C. Y. Jim, W. Y. Chan et al. the effects of different materials and colors of roofs on solar reflection and radiative cooling were mainly studied. The team selected a variety of common roofing materials, tested their reflectance and emissivity, and analyzed their thermal performance under different seasonal and climatic conditions. The results show that roofs with high reflectance and emissivity can effectively reduce heat absorption and lower indoor temperatures, thus improving the thermal comfort of buildings. Meanwhile, W. S. Cai, G. Li et al. investigated a passive radiant cooling technology capable of achieving lower than ambient temperatures under direct sunlight [16]. The research team designed a novel radiative cooling surface that achieves efficient infrared radiation emission and sunlight reflection by optimizing the material structure and spectral selectivity. The experimental results show that this radiation cooling surface can reduce the temperature below the ambient temperature under direct sunlight, which provides a new idea for energy efficient radiation cooling technology [17].

Based on the above literature, it can be seen that the efficiency of radiative cooling can be greatly enhanced by improving the scattering efficiency of sunlight, so exploring the influencing factors of the scattering efficiency of sunlight will play an important role in the research of radiative cooling.

1.4.2. Factors affecting solar reflectance

Wang Tong et al. [18] in their study of the factors affecting solar reflectivity found that the close arrangement of micro- and nanoscale pores on the surface of $PMMA_{HPA}$ film maximises the surface area and the number of scatterers per unit area, thereby increasing the overall scattering efficiency, especially in the near-infrared to short-wave infrared range. Experimental and theoretical studies have shown that the solar reflectance of $PMMA_{HPA}$ thin film is related to the pore size and porosity. In experiments, the solar reflectance of $PMMA_{HPA}$ thin film varies with the aperture diameter. For example, $PMMA_{HPA}$ thin film with a pore size of about 200-300 nm has the highest solar reflectivity. In addition, the solar reflectance of $PMMA_{HPA}$ films are positively correlated with the porosity.

Zeyu Ren [19] at Donghua University found that when increasing the compressive deformation of MTMS crosslinked CNF composite aerogel material (M-CNFA), the reflectivity also increases and can reach 97%. This is due to the fact that compression makes the pore size decrease and the pore wall folds become more, increasing its reflection and scattering of sunlight. Therefore, it can be concluded that the change of pore structure affects the reflectivity of sunlight, and the decrease of pore size and the increase of pore wall folds can increase the reflectivity of sunlight.

Chen Xi [20] of Southeast University found that adjusting the distribution of holes can change the reflectivity of composite films. By controlling the parameters such as the size, shape and distribution density of the holes, the scattering and reflecting effects of the composite film on sunlight can be adjusted, thus changing its reflectivity. For example, the reflectivity of pure PLA film reaches 95%, which is due to the strong Mie scattering induced by the proper fiber size and irregular pore diameter, which enhances the reflection effect.

Therefore, in the preparation of porous film if you can reasonably adjust the pore structure, fiber size and change the shape of the scattering cross-section, you can enhance the reflective effect, to achieve a better effect of radiation cooling.

1.5. Current Vacancies in the Structure of Shaped Pores on the Efficiency of Light Scattering in Radiative Cooling

Although some progress has been made in the research on the application of porous materials in radiative cooling, there are still gaps in the more detailed research on the porous structure and reflectivity in daytime radiative cooling. Particularly in designing shaped structures to improve light scattering efficiency, the prevailing shapes used in designing radiative cooling materials at home and abroad are now simplified to circular or spherical structures, e.g., Benoit Rousseau [21] et al. investigated the role of the texture of porous semi-transparent materials consisting of polydispersed and disjointed spherical pores on their thermal radiative properties, but the role of more complex shapes (ellipsoidal However, more complex shapes (ellipsoidal, cylindrical, polyhedral) have not been addressed, and the effect of a heterogeneous cross-section has been neglected in this study. In the shape optimization of dielectric nanorods for strong directional scattering written by Juan C. Araújo, the benefits of heterogeneous shapes for solar scattering are presented and experimentally demonstrated [22], but the heterogeneous shapes have not been incorporated into the fabrication of radiatively cooled materials. The design of these shaped structures often has a significant impact on the light scattering efficiency, which affects the effectiveness of radiative cooling. Therefore, how to optimize the heteromorphic structure to improve the light scattering efficiency is one of the important challenges facing the current application of porous membranes in the field of radiation cooling.

Therefore, this project will be based on cellulose acetate porous membrane by comparing and analyzing the size and roughness of different heteromorphic cross sections to find the heteromorphic shapes with better scattering efficiency as a way to prepare better materials for radiation cooling.

2. THEORETICAL AND ANALOG SIMULATION MEASUREMENTS OF PARTICLE OPTICAL PROPERTIES

2.1. Light Scattering from Particles

Scattering of light mainly refers to when light passes through some medium inhomogeneous space, due to the uneven refractive index of the medium causes the incident light to deviate from the original direction of incidence, in which all the formulas and phenomena involved in classical optics are based on the mathematical basis of Maxwell's (Maxwell's) system of equations [23] as shown in Eq. (2):

$$\begin{cases} \nabla \cdot D = \rho \\ \nabla \times E = -\frac{\partial B}{\partial t} \\ \nabla \cdot B = 0 \\ \nabla \times H = J + \frac{\partial D}{\partial t} \end{cases} \tag{2}$$

In the above equation, ∇ is the Hamiltonian operator, D is the potential shift vector, ρ is the charge density, E is the electric field vector, B is the magnetic induction vector, H is the magnetic field vector, and J is the current density vector. Any accurate method of electromagnetic scattering is an explicit solution obtained from solving Maxwell's equations in either the time or frequency domain.

According to the theory of Maxwell's equations, when electromagnetic radiation interacts with tiny particles with positive and negative charges in the atmosphere, these particles act as secondary sources of radiation, scattering electromagnetic waves in all directions. This scattering phenomenon is not only related to the size, shape and refractive index of the particles, but is also affected by the wavelength, intensity and polarization state of the incident light. Usually, we take the dimensionless size parameter x=kr as a quantization criterion, where r is the equivalent radius of the particle, and $k=2\pi/\lambda$ represents the wave number, where λ is the wavelength of the incident wave. According to the sizes of different size parameters x, the scattering can be classified into three categories, as shown in the figure below:

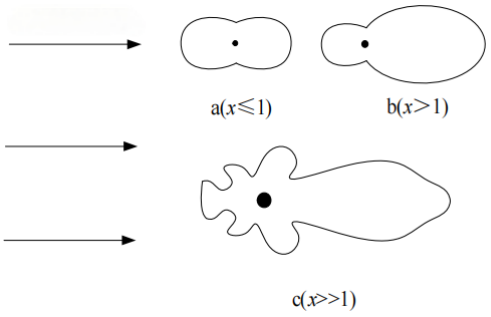

Figure 2. Scattering direction of particles with different size parameters

As shown in the figure, when x≤1 is Rayleigh scattering, when x≥1 is Mie scattering; when x≫1 is the geometrical optics scattering of the particle. When the particle size parameter is less than or equal to 1, the scattering direction of the particles is uniform, and when the particle size parameter gradually increases, the scattering intensity of the particles will also gradually increase. In this paper, the scattering of cellulose acetate film particles with size parameter greater than 1 is mainly studied and analyzed.

2.2. Mie Scattering Theory

Mie theory, also known as Mie scattering theory, was derived by the German physicist Gustav Mie in the early 1900s (1908) using Maxwell's equations to obtain a rigorous solution for elastic scattering by a uniform medium sphere. As shown in Figure 3, when the incident electromagnetic wave is

incident along the z coordinate direction, the center of the particle sphere of radius r is located at the origin of the coordinate axis, the electric vector is polarized in the direction of the x coordinate axis, the distance of the observation position p point from the origin is r, and the plane composed of p point and the coordinate axis z is the scattering surface.

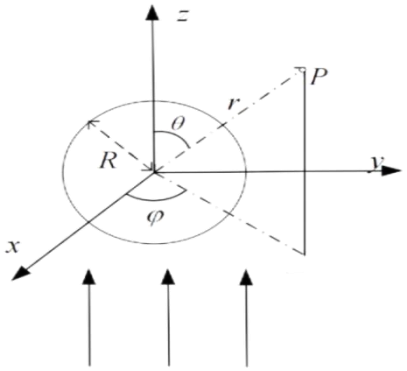

Figure 3. Schematic diagram of Mie scattering theory

Assuming that the light intensity isI_{in}, the scattered fieldI_{sca} received at point p can be expressed by equation (3):

$$I_{sca} = I_{in}\frac{I(\theta,\varphi)}{k^2r^2} \tag{3}$$

$$\mathrm{I}(\theta,\varphi) = |\mathrm{S}_1(\theta)^2|\sin^2\varphi + |\mathrm{S}_2(\theta)^2|\cos^2\varphi \tag{4}$$

Where k is the wave number, θ is the scattering angle of the particle, φ is the polarization angle consisting of the incident light and the scattering surface, $\mathrm{S}_1(\theta)$ and $\mathrm{S}_2(\theta)$ are the polarization functions, and the main equations are as follows:

$$\mathrm{S}_1(\theta) = \sum_{\mathrm{n}=1}^{\infty}\frac{2\mathrm{n}+1}{\mathrm{n}(\mathrm{n}+1)}[\mathrm{a}_\mathrm{n}\pi_\mathrm{n} + \mathrm{b}_\mathrm{n}\tau_\mathrm{n}] \tag{5}$$

$$\mathrm{S}_2(\theta) = \sum_{\mathrm{n}=1}^{\infty}\frac{2\mathrm{n}+1}{\mathrm{n}(\mathrm{n}+1)}[\mathrm{a}_\mathrm{n}\tau_\mathrm{n} + \mathrm{b}_\mathrm{n}\pi_\mathrm{n}] \tag{6}$$

Where a_n and b_n are the Mie scattering coefficients, both of which are related to the negative refractive index m and the size parameter x only, and π_n and τ_n are related to θ only as a function of the scattering angle, so in this paper, if we want to carry out the solving of $\mathrm{S}_1(\theta)$ and $\mathrm{S}_2(\theta)$ first, we have to solve for a_n and b_n, π_n and τ_n first, where the formulas for a_n and b_n, π_n and τ_n are as follows:

$$\mathrm{a}_\mathrm{n} = \frac{\psi_\mathrm{n}(\mathrm{x})\psi_\mathrm{n}'(\mathrm{mx}) - \mathrm{m}\psi_\mathrm{n}'(\mathrm{x})\psi_\mathrm{n}(\mathrm{mx})}{\xi_\mathrm{n}(\mathrm{x})\psi_\mathrm{n}'(\mathrm{mx}) - \mathrm{m}\xi_\mathrm{n}'(\mathrm{x})\psi_\mathrm{n}(\mathrm{mx})} \tag{7}$$

$$\mathrm{b}_\mathrm{n} = \frac{\mathrm{m}\psi_\mathrm{n}(\mathrm{x})\psi_\mathrm{n}'(\mathrm{mx}) - \psi_\mathrm{n}'(\mathrm{x})\psi_\mathrm{n}(\mathrm{mx})}{\mathrm{m}\xi_\mathrm{n}(\mathrm{x})\psi_\mathrm{n}'(\mathrm{mx}) - \xi_\mathrm{n}'(\mathrm{x})\psi_\mathrm{n}(\mathrm{mx})} \tag{8}$$

$$\pi_\mathrm{n} = \frac{\mathrm{P}_\mathrm{n}^1(\cos\theta)}{\sin\theta} = \frac{\mathrm{dP}_\mathrm{n}(\cos\theta)}{\mathrm{d}\cos\theta} \tag{9}$$

$$\tau_\mathrm{n} = \frac{\mathrm{dP}_\mathrm{n}^1(\cos\theta)}{\mathrm{d}\theta} = -\mathrm{P}_\mathrm{n}^1(\cos\theta)\sin\theta \tag{10}$$

Where $\psi_n(x)$ and $\xi_n(x)$ in Eqs. (7), (8) are functions of half-order integer Bessel functions and Hankel functions of the second kind, respectively, $\psi_n'(x)$ and $\xi_n'(x)$ are first-order derivatives of $\psi_n(x)$ and $\xi_n(x)$, respectively, $P_n^1(\cos\theta)$ and $P_n(\cos\theta)$ are first-order nth-order first-type concatenated Legendre (Legendre) functions, respectively, and the complex refractive index m = n + ki is a complex number. After obtaining the parameters such as scattering coefficient and scattering amplitude function, the particle scattering efficiency factor (Qsca), extinction efficiency factor (Qext), absorption efficiency factor (Qabs), scattering cross-section (Csca), extinction cross-section (Cext), absorption cross-section (Cabs), backward scattering efficiency factor (Q), asymmetry factor (g), and single albedo (ω) can be computed scattering characteristics [24], the specific expressions are shown below:

$$Qsca = \frac{2}{x^2}\sum_{n=1}^{\infty}(2n+1)(|a_n|^2 + |b_n|^2) \tag{11}$$

$$Qext = \frac{2}{x^2}\sum_{n=1}^{\infty}(2n+1)\{Re(a_n + b_n)\} \tag{12}$$

$$Qabs = Qext - Qsca \tag{13}$$

$$Csca = \frac{\lambda^2}{2\pi}\sum_{n=1}^{\infty}(2n+1)(|a_n|^2 + |b_n|^2) \tag{14}$$

$$Cext = \frac{\lambda^2}{2\pi}\sum_{n=1}^{\infty}(2n+1)\{Re(a_n + b_n)\} \tag{15}$$

$$Cabs = Cext - Csca \tag{16}$$

$$Q = \frac{1}{x^2}\left|\sum_{n=1}^{\infty}(2n+1)(-1)^n(a_n - b_n)\right| \tag{17}$$

$$g = \frac{4}{x^2 Qsca}\sum_{n=1}^{\infty}\frac{n(n+1)}{n+1}\left[Re(a_n a_{n+1}^* + b_n b_{n+1}^*) + \frac{2n+1}{n(n+1)}Re(a_n b_n^*)\right] \tag{18}$$

$$\omega = \frac{Csca}{Cext} \tag{19}$$

From equations (2-12) and (2-13), we can get Cext=GQext, G represents the cross-sectional area of the particle in the same direction as the incident wave ($G = \pi R^2$ for spherical particles, R is the radius of the particle of equal volume).

G represents the cross-sectional area of the particle in the same direction as the incident wave (in the case of spherical particles, $G = \pi R^2$, R is the radius of the particle of the same volume), Qext, Qabs and Qsca describe the physical quantities of the efficiency of the particles to extinguish, scatter and absorb the incident light, and Cext, Cabs and Csca describe the physical quantities of the energy attenuation of the energy dissipated by scattering of a particle under the irradiation of the incident light. The physical quantity of scattering efficiency in the opposite direction of incident light is expressed by the backward scattering efficiency factor Q. The asymmetry factor g expresses the meaning of the symmetry between forward and backward scattering of a particle, and the single scattering albedo ω expresses the share of scattering in the extinction, which shows the particle's scattering ability [25].

As shown in the following figure, the trend of each scattering parameter of the spherical particles with complex refractive index m=1.4947+0.0075i calculated according to the above Mie theoretical formula is given with the increase of the size parameter. It can be seen that the first peak of the extinction efficiency factor occurs near x = 4, and then decays and oscillates between 2-2.5 with the increase of the size parameter; the maximum value of the backward scattering efficiency factor occurs

at x = 9, and then gradually decreases and tends to be close to 0 with the increase of the particle size parameter.

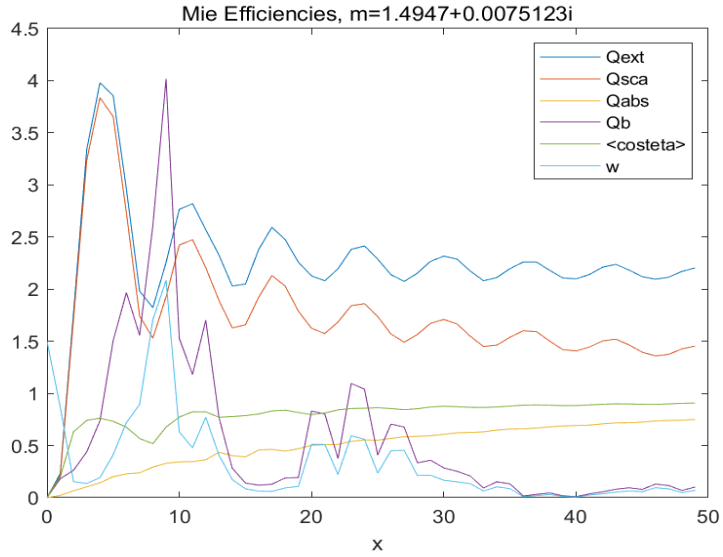

Figure 4. Variation of scattering characteristics with size parameter for complex refractive index of m=1.4947+0.0075i

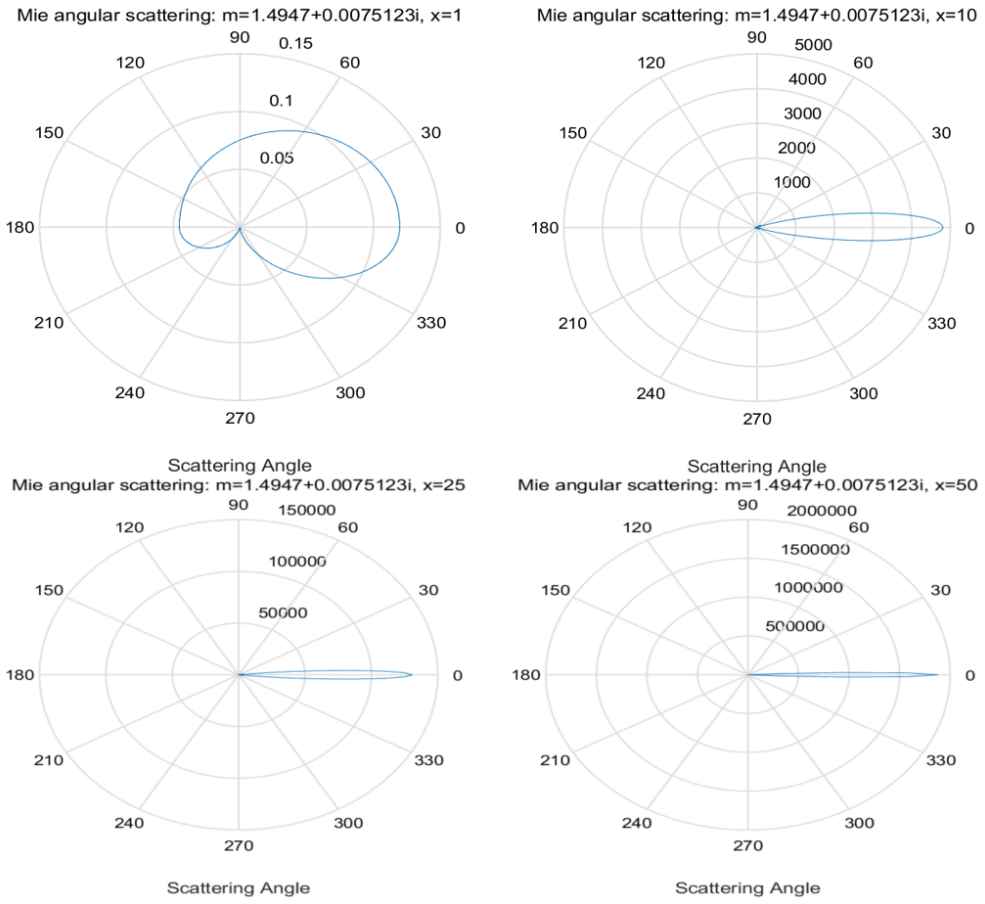

Figure 5. Scattering direction of the same particle with different size parameters

Figure 5 shows the trend of the scattered light intensity of the spherical particles with the size parameter from 1 to 50 for the theoretically calculated complex refractive index m=1.4947+0.0075i, and it can be seen that the larger the size parameter of the particles is, the more the scattered direction

of the particles is concentrated in the front direction and the intensity of scattering is larger, and the intensity of the backward scattered light intensity is smaller, even approaching to 0. Moreover, the size parameter is not only related to the equivalent radius of the particles, but also related to the incident wavelength. and the wavelength of incident light. When the size parameter is larger, the scattering direction is more concentrated.

3. SHAPED SHAPES

3.1. Classification of Shaped Shapes

Shaped fibers refer to those fibers that are different from round fibers and have a specific non-round cross-section shape. This type of fiber is an important branch in the field of differentiated fibers. Fiber heteromorphism is a method of physical modification of fiber cross-section to obtain different fiber properties [26], which is an important means of preparing heteromorphic fibers and one of the key technologies for preparing heteromorphic fibers. The classification of fiber cross-section morphology is shown in Figure 6 [27], and fiber heteromorphization is mainly divided into two main categories: one is the heteromorphization of fiber cross-section shape, including contour fluctuation and diameter asymmetry; and the other is the hollowing and composite of fiber cross-section. With the increasing number of methods for fiber cross-section deformations, researchers have successfully developed a variety of deformed fibers, such as triangular, metric, C-shaped, hollow and orange-flap shapes. Usually, the fiber cross-section is shaped to enhance the performance of the fiber in certain aspects, thus expanding its application areas.

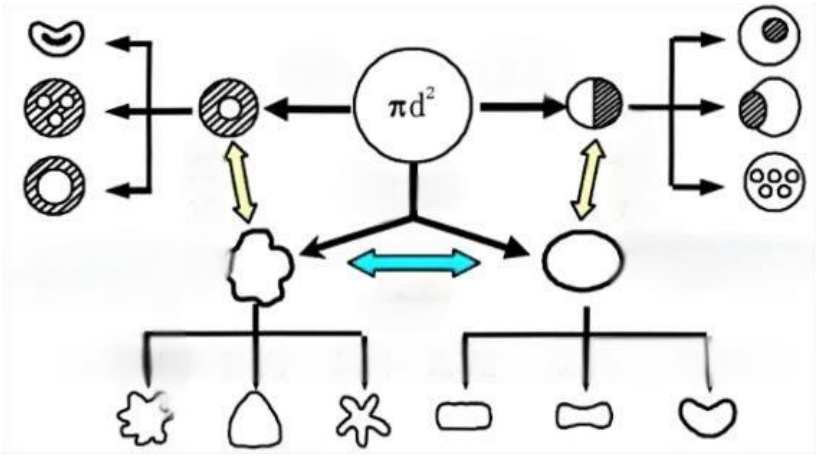

Figure 6. Classification of cross-sectional morphology of fibers

With the development of fiber cross-section isomorphization technology, fiber isomorphization has been extended from only changing the fiber diameter to the degree of changing the fiber profile; hollow fibers from the original single-pore isomorphism further developed into porous isomorphism, and also from the single-component fibers further evolved into multi-component fibers. Therefore, the progress of fiber heteromorphism technology makes chemical fibers no longer have the problem of performance defects and single function, but toward the direction of performance diversification and multifunctionality [28]. And the object studied in this paper is the shape of contour fluctuation heteromorphism based on Fourier variation.

3.2. Modeling of Heteromorphic Shapes

In this paper, the modeling of shaped shapes is carried out according to the Fourier formula, which is as follows:

$$R(\theta) = r + \sum_{i=0}^{N}(\alpha_{2i-1}\cos(i\theta) + \alpha_{2i}\sin(i\theta)) \quad (20)$$

Where r is the circular circular radius, N is the degree of deviation, the larger the value of N, indicating that the higher the degree of deviation from the circle, the more pronounced the degree of heteromorphism, the above formula is converted to polar coordinates as:

$$x = (R + \sum_{i=0}^{16}(r_i * \cos(i * t) + r_{i+1} * \sin(i * t))) * \cos(t) \quad (21)$$

$$y = (R + \sum_{i=0}^{16}(r_i * \cos(i * t) + r_{i+1} * \sin(i * t))) * \sin(t) \quad (22)$$

Where the modeled alien shape is:

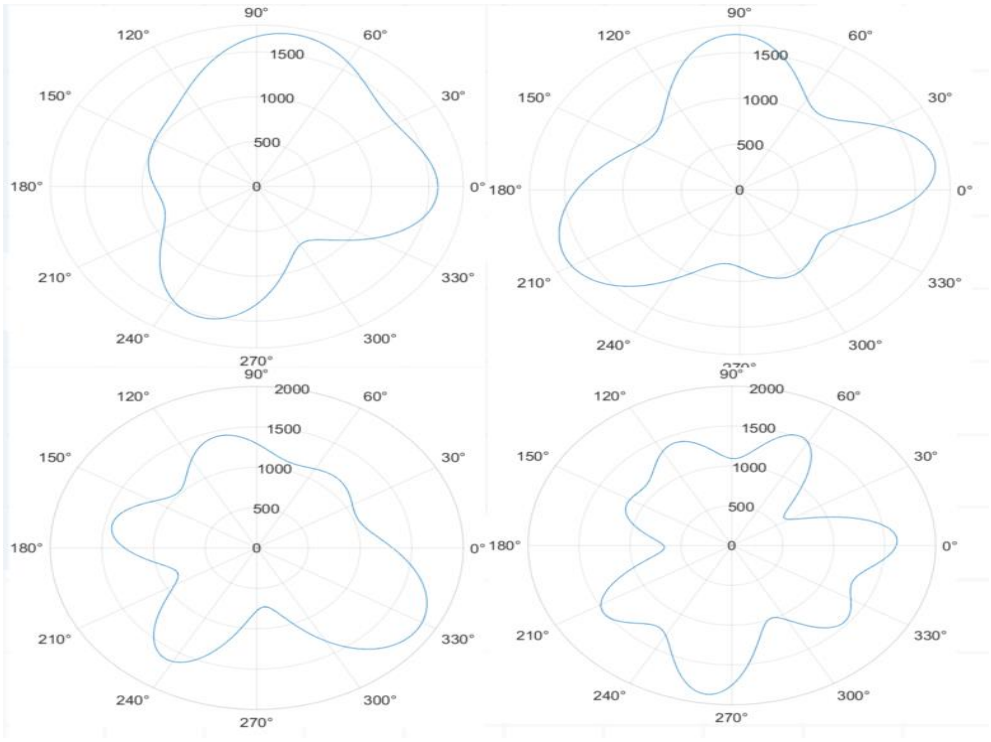

Figure 7. Simulation effect of shaped shapes (N=4-8)

3.3. Experimental Simulation

In order to study the effect of the heteromorphic shape on the optical performance, this paper uses the comsol version of the software for the construction of the physical field and the simulation of the scattering efficiency of the heteromorphic shape.In this paper, we use the frequency-domain module of fluctuating optics of comsol itself for the construction of the physical field and use the two-dimensional model of the Mie scattering simulation to calculate the optical performance of the heteromorphic shape of the cellulose acetate based porous material.

In this paper, the relationship between the size and the degree of heteromorphism of the heteromorphic shape and the scattering efficiency is calculated from the 2D simulation model constructed with the heteromorphic shape (cellulose acetate membrane) under a circular boundary (air layer) and compared with the circular shape, which leads to the conclusion that the scattering efficiency of the heteromorphic shape is stronger than that of the circular shape under the same conditions. For waves, in this paper, according to the comsol fluctuating optics module, plane waves with wavelengths of 300--2500 nm are used with one step length per 5 nm, and the model is constructed by applying the frequency-domain module of the scattering electric field and setting it to propagate along the y-axis in the positive direction in the plane of incidence, and also using the x-axis as the perfect matching layer (PML) boundary condition of the PML. During the comsol simulation, the dimensions of the air layer in the simulation model are set as a circle with a radius of

2000 nm in this paper. The incident light is 300-2500 nm, and finally the one-dimensional map group and two-dimensional scattering field of the scattering efficiency of the shaped shape are obtained according to the comsol calculation.

The specific experimental results are shown in Fig. 8:

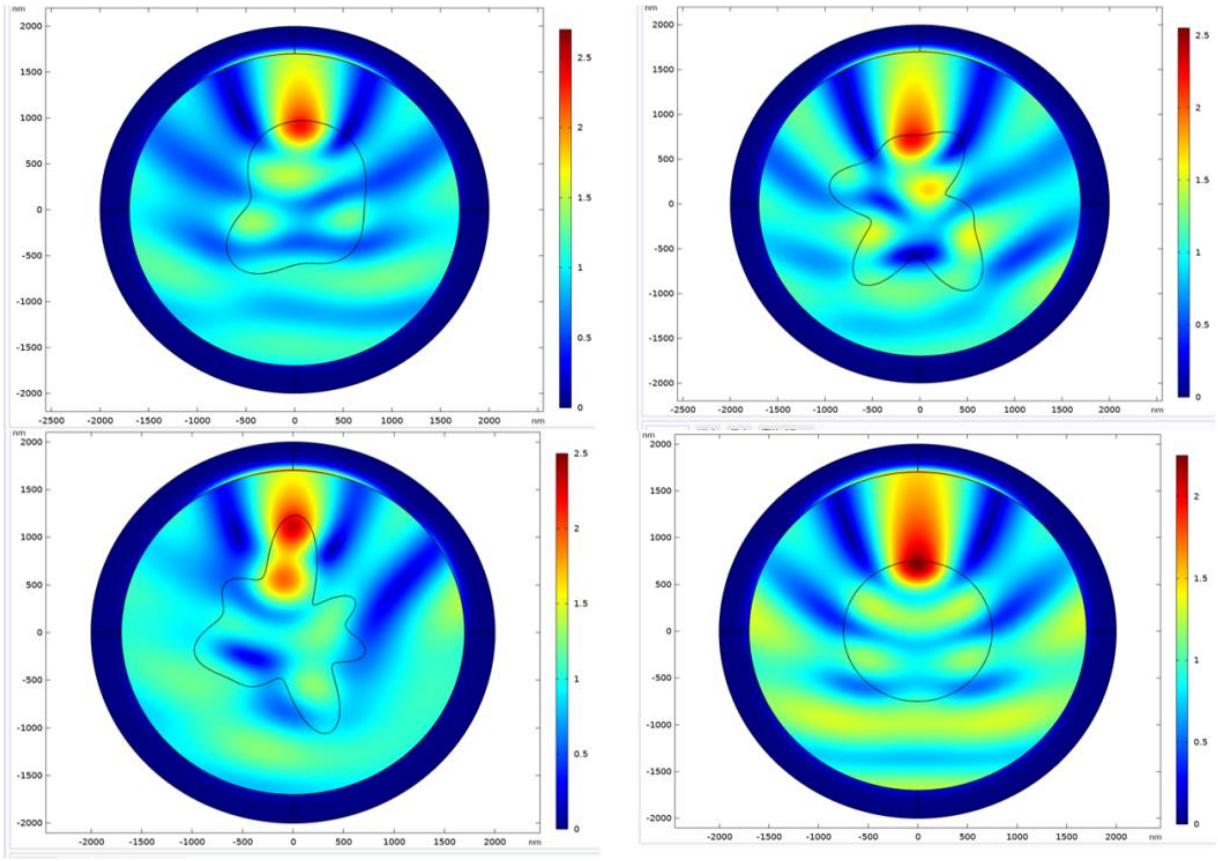

Figure 8. Comparison of scattering cross section of shaped shape and circular shape

As can be seen in the figure, the electric field strength (represented by the colors) varies significantly at different locations. The red areas represent higher electric field strengths, while the blue areas indicate lower electric field strengths. The shapes in the center represent different shapes of the particle cross-section respectively, mainly a comparison between circular and heterogeneous shapes, and the surrounding color pattern demonstrates the variation of the electric field strength with space, and it can be seen that among the heterogeneous shapes, the electric field strength of the heterogeneous shapes is higher than that of the circular shapes on the whole, and, thus, it can be seen that the heterogeneous shapes have a higher scattering effect compared with circular shapes because of the heterogeneous shapes have a bigger The reason for the higher scattering effect of heteromorphic shapes compared to circular shapes is that heteromorphic shapes have a larger surface area than circular shapes, and their special and irregular shapes can form asymmetric scattering routes when scattering light, so that the light can be better scattered from the side.

4. SUMMARY

In this paper, we mainly take the highly flexible and moldable cellulose acetate as the research object, and use the Mie scattering formula to simulate the calculation, mainly through the measured complex refractive index of cellulose acetate film into the formula, and then find out the different sizes of cellulose acetate film scattering efficiency, absorption efficiency, extinction efficiency, backward scattering efficiency factor and other changes in the size of the trend, and then, in the next to investigate the effect of different parameters on the scattering direction. Subsequently, the effect of

different parameters on the scattering direction was investigated, and it was found that the scattering direction was gradually concentrated with the increase of the size parameter. On this basis, the reduced modeling and simulation of the shaped shapes of cellulose acetate films are carried out, and it is found that the electric field strengths of the shaped shapes are higher than those of the circular shapes, which confirms that the shaped shapes have a higher scattering effect compared with the circular shapes, and thus provide feasible graphic schemes and proofs for the shaped shapes of cellulose acetate films.

REFERENCES

[1] Raman, A. P., Anoma, M. A., Zhu, L., Rephaeli, E. & Fan, S. Passive radiative cooling below ambient air temperature under direct sunlight. Nature 515, 540 -- 544 (2014)

[2] Lv Song; Ji Yishuang; Ji Yitong; Qian Zuoqin; Ren Juwen; Zhang Bolong; Lai Yin; Yang Jiahao; Chang Zhihao.Experimental and numerical comparative investigation on 24h radiative cooling performance of a simple organic composite film. Journal | [J] Energy. Volume 261, Issue PA. 2022.

[3] W. Lu et al., Porous membranes in secondary battery technologies. Chemical Society Reviews 46, 2199-2236 (2017).

[4] Yuan Shuaixia. Preparation and application of natural cellulose based daytime passive radiation refrigeration materials.

[5] Chen Xi. Cellulose-based porous polymer film with auto-deposited TiO_2 as spectrally selective materials for passive daytime radiative cooling. Optical Materials Volume 120, October 2021, 111431.

[6] Jia Jianru. Study on modification and properties of cellulose acetate nanofiber membrane.

[7] Feng M, Feng S, Liu C, et al. Integrated passive cooling fabrics with bioinspired perspiration-wicking for outdoor personal thermal management [J]. Composites Part B: Engineering, 2023, 264: 110875.

[8] Zhang K, Mo C, Tang X, et al. Hierarchically Porous Cellulose-Based Radiative Cooler for Zero-Energy Food Preservation [J]. ACS Sustainable Chemistry & Engineering, 2023, 11(20):7745-7754.

[9] Zheng Y, Zhu Y, Yu Z, et al. Passive thermal regulation with 3D printed phase change material/cellulose nanofibrils composites [J]. Composites Part B: Engineering, 2022, 247: 110332.

[10] Li T, Zhai Y, He S, et al. A radiative cooling structural material [J]. Science, 2019, 364(6442): 760-763.

[11] ZHU Jia, WANG Minghuai "Protecting ice from melting under sunlight via radiative cooling".

[12] Chen Xi Study on preparation and cooling performance of passive daytime radiative cooling film.

[13] Wei Wei, Yong Zhu, Qiu LiAn Al_2O_3-cellulose acetate-coated textile for human body cooling.

[14] Yuxin Zhang, Dingsheng Wu, Shiqin Liao A multi-mode cellulose acetate/MXene Janus film with structure enhanced self-reflection, selective emission and absorption for cooling and heating.

[15] Chen Si, Yang Xujie Design and properties of radiative cooling materials based on spectral selectivity.

[16] C. Y. Jim, W. Y. Chan, et al."Solar Reflectance and Thermal Emissivity of Cool Roofs".

[17] W. S. Cai, G. Li, et al. "Passive radiative cooling below ambient air temperature under direct sunlight".

[18] Tong Wang, Yi Wu, Lan Shi, et, al. A structural polymer for highly efficient all-day passive radiative cooling. Nature Communications, 2021, 12 (1) : 365.

[19] Ren Zeyu. [19] Preparation of cellulose nanofiber composite aerogel and its daytime radiation refrigeration performance.

[20] Chen Xi. Cellulose-based porous polymer film with auto-deposited TiO2 as spectrally selective materials for passive daytime radiative cooling. Optical Materials Volume 120, October 2021, 111431.

[21] Benoit Rousseau, Domingos De Sousa Meneses, Patrick Echegut, Jean-Francois Thover. Textural parameters influencing the system radiative properties of a semitransparent porous media. International Journal of Thermal Sciences 50 (2011) 178e186.

[22] Juan C. Araujo, Eddie Wadbro, Shape optimization for the strong directional scattering of dielectric nanorods.

[23] Yang Guoguang, Song Feijun. Advanced Physical Optics [M]. University of Science and Technology of China Press, 2008.

[24] HOU Honglu, Liu Kai, Zhao Qunying. Numerical simulation of light scattering properties of soot aerosols [J]. Journal of Xi 'an Technological University, 2016, 36(09): 719-725.

[25] Gao Tian-Le. Correction and fusion of aerosol active and passive detection for oblique visibility [D]. Xi 'an University of Technology, 2020. (in Chinese)

[26] Han Yingbo, Xu DeZeng, CAI Yuefen, et al. [26] Discussion on modification method of polyester fiber [J]. Polyester Industry, 2003, 16 (2) : 11-14. HAN Yingbo, XU Dezeng, CAI Yuefen, et al. Discussion on modified methods of polyester [J]. Polyester Industry, 2003, 16(2): 11-14.

[27] Liu Lu. Optimal design of nonwoven air filtration materials: Influence of fiber morphology [D]. Tianjin: Tianjin Polytechnic University, 202:1-2. (in Chinese) LIU Lu. Optimal Design of Nonwoven Air Filter Materials: The Influence of Fiber Morphology [D]. Tianjin: Tianjin Polytechnic University, 2021: 1-2.

[28] Wang Huiyun. [28] Preparation and properties of polyacrylonitrile fiber with triangular polyspace [D]. Suzhou: Soochow University, 202:2. WANG Huiyun. Preparation of PAN Triangular Hollow Porous Fiber and Its Performance [D]. Soochow University, 2021: 2.